Supplementary Information

Formic acid dehydrogenation over PdNi alloys supported on N-doped carbon: Synergistic effect of Pd-Ni alloying on hydrogen release

Rizcky Tamarany,[#,a] Dong Yun Shin,[#,b] Sukho Kang,[b] Hyangsoo Jeong,[a] Joohoon Kim,[c,d] Jun Kim,[a] Chang Won Yoon,[*,a,c] and Dong-Hee Lim[*,b]

[a]Center for Hydrogen and Fuel Cell research, Korea Institute of Science and Technology (KIST), 5 Hwarang-ro 14-gil, Seongbuk-gu, Seoul 02792, Republic of Korea

[b]Department of Environmental Engineering, Chungbuk National University, Chungdae-ro 1, Seowon-gu, Cheongju, Chungbuk 28644, Republic of Korea

[c]KHU-KIST Department of Converging Science and Technology, Kyung Hee University, 26 Kyungheedae-ro, Dongdaemun-gu, Seoul 02447 Republic of Korea

[d]Department of Chemistry, Research Institute for Basic Sciences, Kyung Hee University, 26 Kyungheedae-ro, Dongdaemun-gu, Seoul 02447, Republic of Korea

[Experimental Part]

[Theoretical Part]

1. Supplementary information: Experimental results

Table S1 The bulk compositions of Pd_1Ni_x/N-C (x = 0, 0.37, 1.3 and 3.6), and Ni/N-C nanoparticles.

Samples	ICP-OES			
	Pd wt%	Ni wt%	Pd/Ni atomic ratio	Ni/Pd atomic ratio
Pd	3.81	-	-	-
$Pd_1Ni_{0.37}$	4.08	0.84	2.68	**0.37**
$Pd_1Ni_{1.3}$	3.78	2.72	0.77	**1.3**
$Pd_1Ni_{3.6}$	3.30	6.53	0.28	**3.6**
Ni	-	3.79	-	-

Table S2 Crystallite sizes of Pd_1Ni_x/N-C (x = 0, 0.37, 1.3 and 3.6) and Ni/N-C calculated using the Scherrer method.[#]

Materials	Peak (2θ)	β (2θ)	L (nm)
Pd/N-C	39.06	2.50	3.52
$Pd_1Ni_{0.37}$/N-C	39.32	2.75	3.20
$Pd_1Ni_{1.3}$/N-C	39.85	2.73	3.23
$Pd_1Ni_{3.6}$/N-C	40.11	3.16	2.79
Ni/N-C	44.38	0.536	16.7

[#]Calculation of crystallite size using Scherrer method

From the well-known Scherrer formula, the average crystallite size (L) is defined as,

$$L = \frac{K\lambda}{\beta \cos\theta}$$

where λ is the X-ray wavelength in nanometer (nm), β is the peak width of the diffraction peak profile at half maximum height resulting from small crystallite size in radians, and K is a constant related to crystallite shape, normally taken as 0.9.

Table S3 XPS Pd_{3d} data for Pd_1Ni_x/N-C (x = 0, 0.37, 1.3 and 3.6).

	Pd^0 (in eV)		Pd^{2+} (in eV)	
Pd/N-C	$Pd_{5/2}$	335.1	$Pd_{5/2}$	-
	$Pd_{3/2}$	340.4	$Pd_{3/2}$	-
$Pd_1Ni_{0.37}$/N-C	$Pd_{5/2}$	335.2	$Pd_{5/2}$	335.9
	$Pd_{3/2}$	340.4	$Pd_{3/2}$	341.1
$Pd_1Ni_{1.3}$/N-C	$Pd_{5/2}$	335.4	$Pd_{5/2}$	336.2
	$Pd_{3/2}$	340.6	$Pd_{3/2}$	341.4
$Pd_1Ni_{3.6}$/N-C	$Pd_{5/2}$	335.6	$Pd_{5/2}$	336.5
	$Pd_{3/2}$	340.8	$Pd_{3/2}$	341.6

Table S4 TOF values for FA dehydrogenation over Pd_1Ni_x/N–C (x = 0, 0.37, 1.3 and 3.6) at different temperatures.

Catalysts	Temperature	TOF (h^{-1})
$Pd_1Ni_{1.3}$/N-C	25 °C	363
	30 °C	447
	45 °C	736
	65 °C	2195
$Pd_1Ni_{0.37}$/N-C	30 °C	369
$Pd_1Ni_{3.6}$/N-C	30 °C	347
Pd/N-C	25 °C	127
	30 °C	232
	45 °C	412
	65 °C	1189
$Pd_1Ni_{1.3}$/C	25 °C	85.5
Pd/C	25 °C	37.5

Table S5 Comparison of Pd based bi- and trimetallic catalysts for formic acid decomposition.

Entry	Catalyst	Temperature (K)	TOF (h^{-1})[a]	Reference
1	Pd_{59} Au_{41}/C	323	230	S1
2	$Pd_{25}Au_{75}$/C	348	212[b]	S2
3	C-$Ag_{42}Pd_{58}$	323	382	S3
4	PdAg-CeO_2	303	322	S4
5	PdNi@Pd/GNs-CB[c]	RT	577[d]	S5
6	$Pd_{0.85}Ir_{0.15}$/SBA-15-NH_2 NCs	298	3,087	S6
7	$Pd_{90}Rh_{10}$/HHT[e]	303	1,793	S7
8	Pd-MnO_x /SiO_2–NH_2	293	140	S8
9	PdNiAg/C	323	85	S9
10	$Pd_1Ni_{0.37}$/N-C	303	369	This work
11	$Pd_1Ni_{1.3}$/N-C	303	447	This work
12	$Pd_1Ni_{3.6}$/N-C	303	347	This work

[a]Determined in a different time; [b]Calculated based on the exposed Pd moles determined using the metallic dispersion obtained by transmission electron microscopy (TEM); [c]GNs-CB, = graphene nanosheets-carbon black; [d]Calculated based on the number of active sites, estimated from hydrogen desorption in H_2SO_4 electrolyte using an electrocatalytic surface area technique; [e]HHT = High Heat Treated carbon nanofibers.

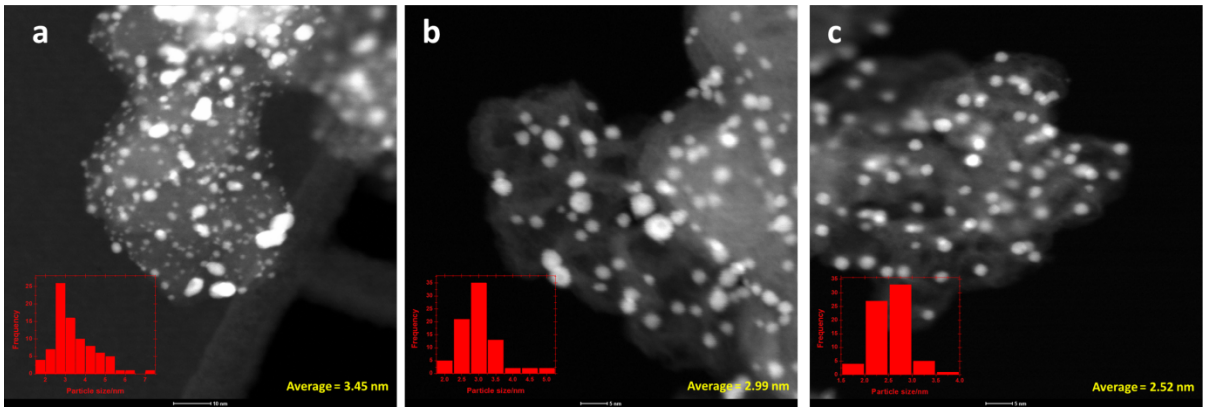

Fig. S1 HAADF–STEM images: (a) Pd/N-C, (b) $Pd_1Ni_{0.37}$/N-C and (c) $Pd_1Ni_{3.6}$/N-C.

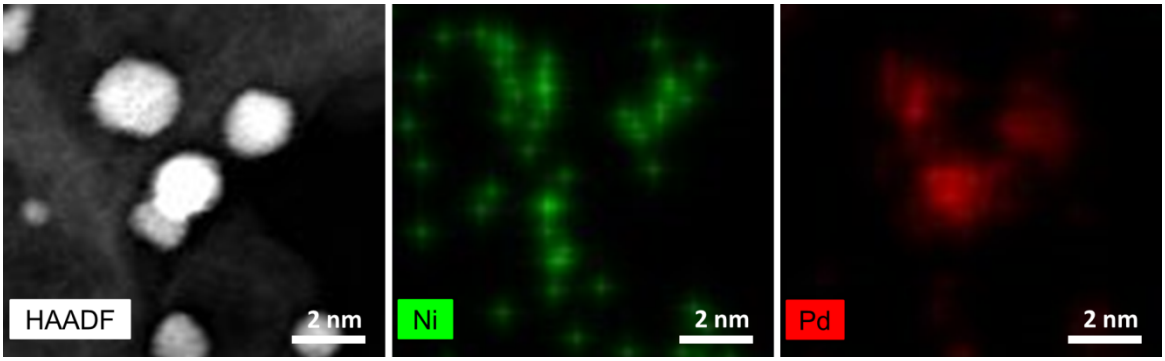

Fig. S2 Elemental mapping for $Pd_1Ni_{1.3}$/N-C catalyst using the high-angle annular dark field scanning TEM (HAADF-STEM).

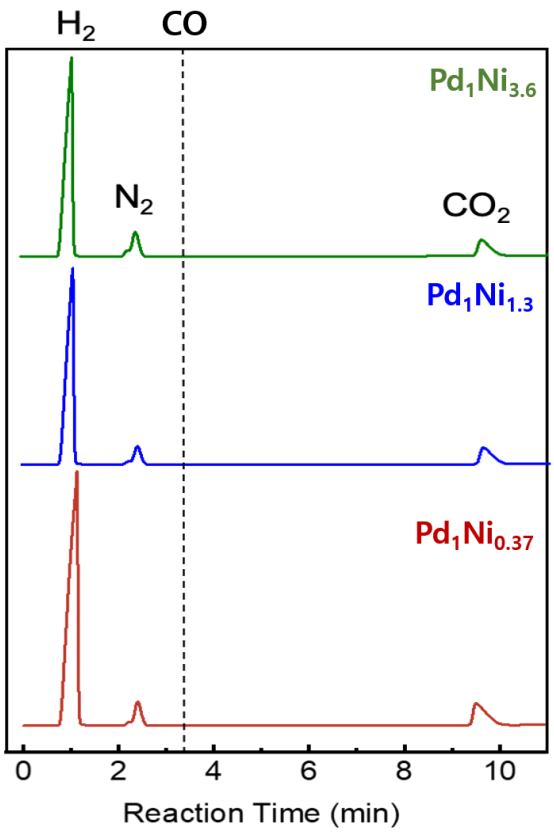

Fig. S3 The GC results with the gases produced from formic acid dehydrogenation: (a) $Pd_1Ni_{0.37}$, (b) $Pd_1Ni_{1.3}$, (c) $Pd_1Ni_{3.6}$. The dotted line indicates the position of CO gas, if released.

2. Supplementary information: Theoretical results

Bulk and surface structures of Pd_1Ni_1 alloy

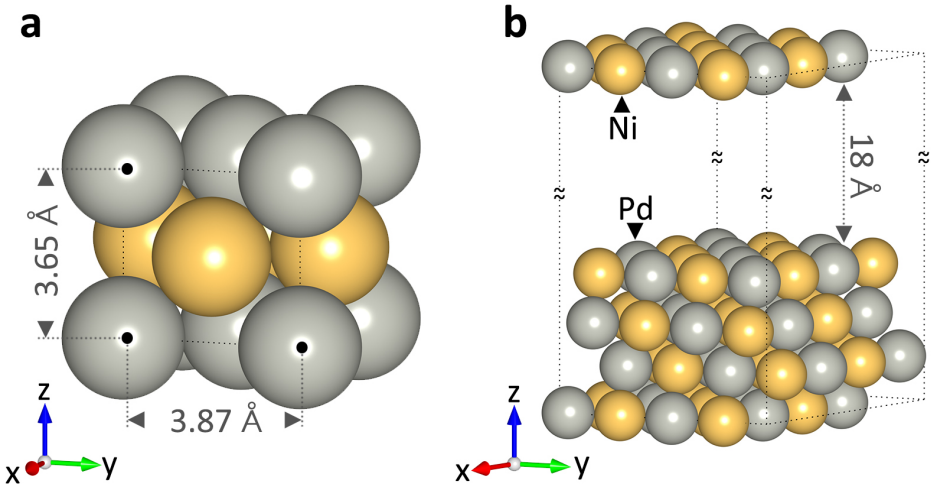

Fig. S4 Side views of (a) bulk fcc Pd_1Ni_1 and (b) Pd_1Ni_1(111) surface model. Grey and light yellow colors represent Pd and Ni, respectively.

Adsorption sites of Pd(111) and Pd_1Ni_x(111) surfaces

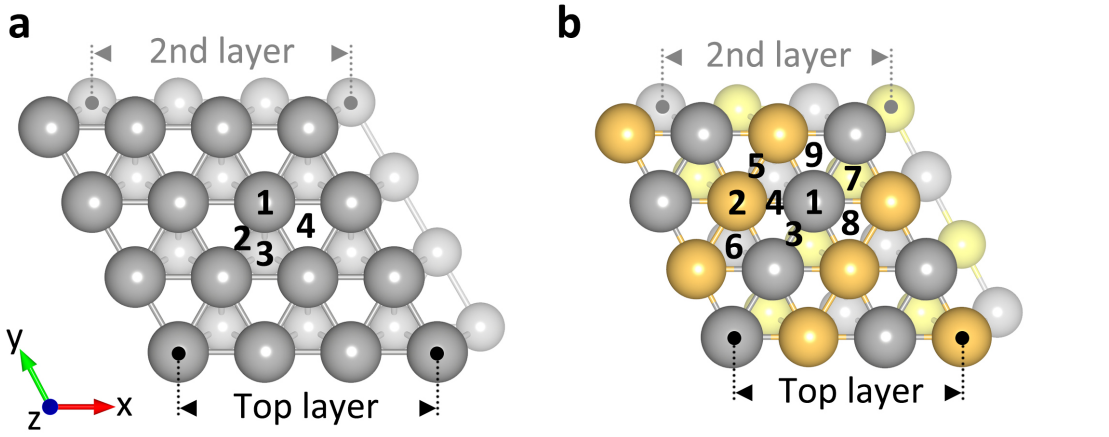

1. atop
2. bridge
3. hollow (hcp)
4. hollow (fcc)

1. atop-Pd
2. atop-Ni
3. bridge-Pd-Pd
4. bridge-Pd-Ni
5. bridge-Ni-Ni
6. hollow (hcp)-Pd_1Ni_2
7. hollow (hcp)-Pd_2Ni_1
8. hollow (fcc)-Pd_1Ni_2
9. hollow (fcc)-Pd_2Ni_1

Fig. S5 Top views of the adsorption sites for (a) Pd(111) and (b) Pd_1Ni_1(111) surfaces.

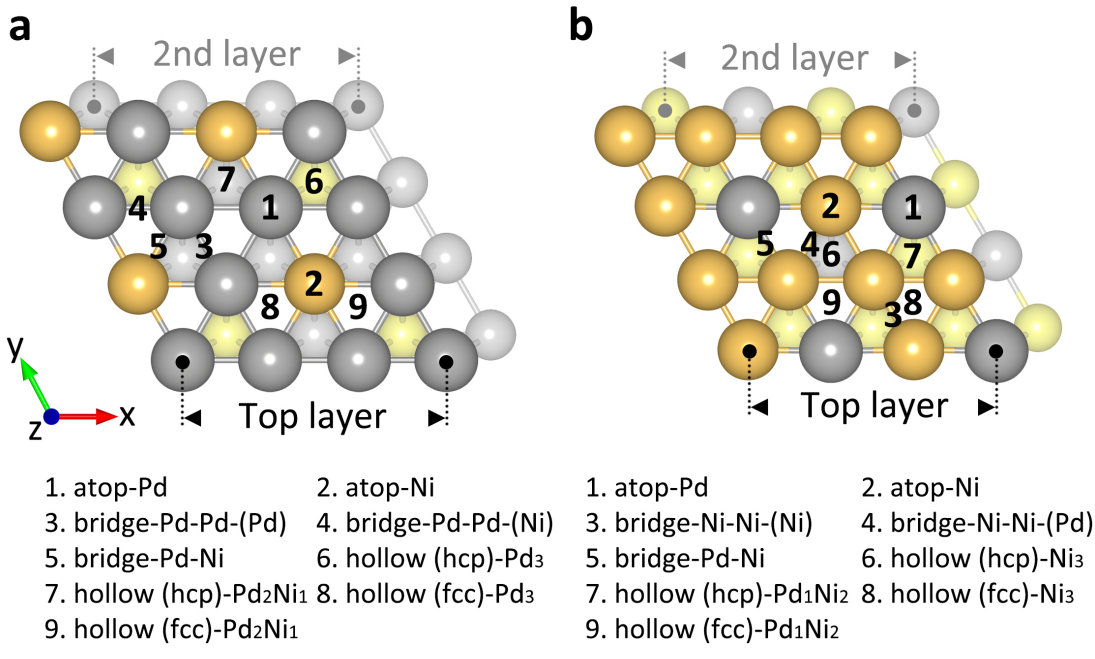

1. atop-Pd	2. atop-Ni
3. bridge-Pd-Pd-(Pd)	4. bridge-Pd-Pd-(Ni)
5. bridge-Pd-Ni	6. hollow (hcp)-Pd_3
7. hollow (hcp)-Pd_2Ni_1	8. hollow (fcc)-Pd_3
9. hollow (fcc)-Pd_2Ni_1	

1. atop-Pd	2. atop-Ni
3. bridge-Ni-Ni-(Ni)	4. bridge-Ni-Ni-(Pd)
5. bridge-Pd-Ni	6. hollow (hcp)-Ni_3
7. hollow (hcp)-Pd_1Ni_2	8. hollow (fcc)-Ni_3
9. hollow (fcc)-Pd_1Ni_2	

Fig. S6 Top views of the adsorption sites for (a) $Pd_1Ni_{0.33}(111)$ and (b) $Pd_1Ni_3(111)$ surfaces.

The most stable adsorption configurations of intermediate species

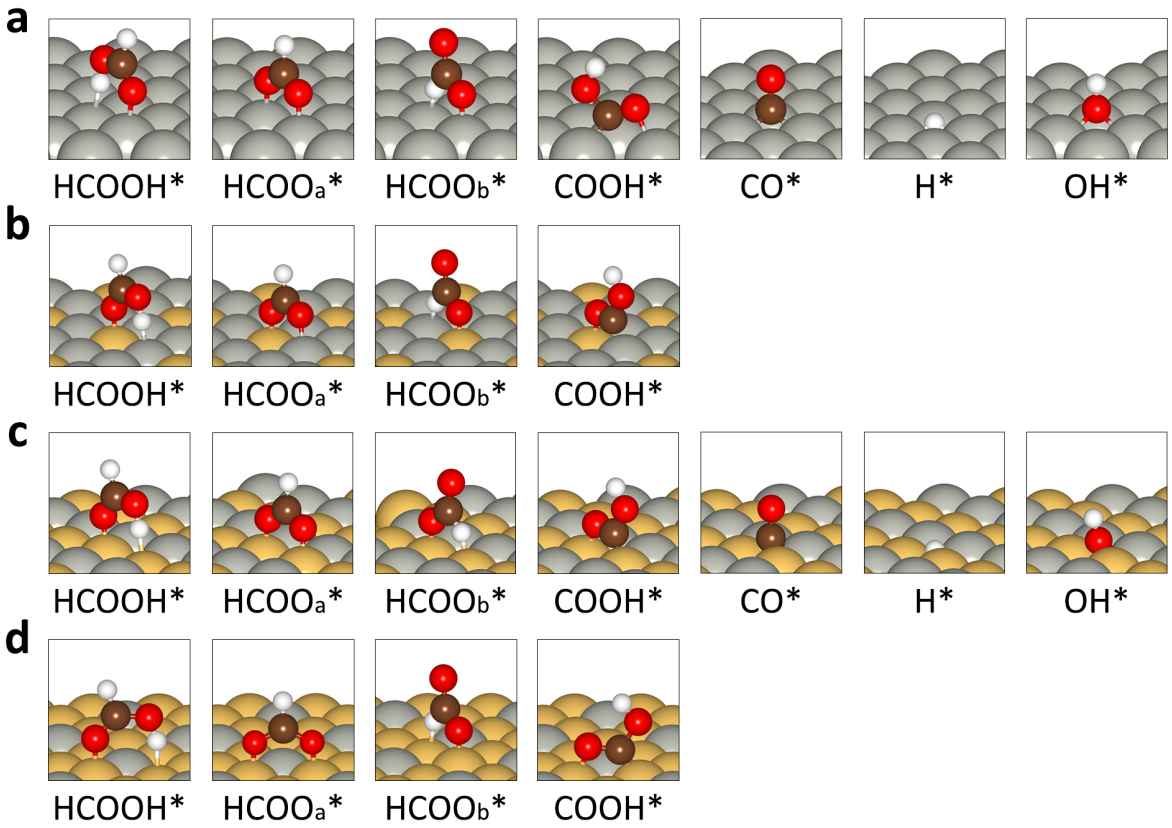

Fig. S7 The most stable adsorption configurations of key intermediate species on (a) Pd(111), (b) $Pd_1Ni_{0.33}$(111), (c) Pd_1Ni_1(111) and (d) Pd_1Ni_3(111) surfaces. Grey, light yellow, dark brown, red and white spheres represent Pd, Ni, C, O and H atoms, respectively.

Spin densities of Pd(111) and Pd_1Ni_x(111) surfaces

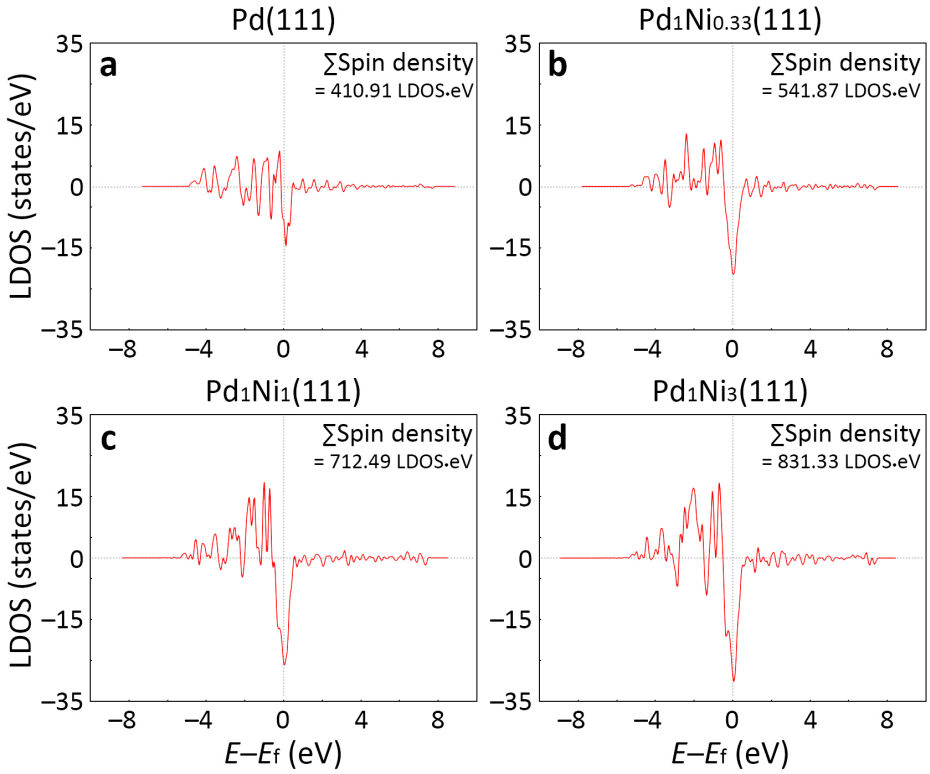

Fig. S8 Spin densities of top layers of Pd(111) and Pd_1Ni_x(111) surfaces. ΣSpin density was calculated by summing the density of spin-up and -down electrons as with the calculation method used in the previous study.[S10]

The spin density can affect catalytic activity related to the adsorption behavior and be used as an indicator for the efficiency of FA dehydrogenation. To verify this, we conducted the non-spin polarized DFT calculation for the adsorption of $HCOO_a$ on Pd_1Ni_1(111) surface using VASP's ISPIN = 1 option (turning off the spin polarization). The adsorption strength of intermediates on the PdNi alloys would be overestimated when spin polarization was turned off. The adsorption energy when the spin option was turned off (–3.42 eV) was stronger than the case when the spin option was turned on (–3.07 eV). This implies that the overestimated adsorption strength would result in an overestimated activation energy of HCOOH dehydrogenation on the PdNi alloys because stronger adsorption of adsorbates would require more energy to be detached and dissociated from the catalytic surface.

The *d*-band centers and spin densities of Pd-Pd and Pd-Ni depending on Ni content

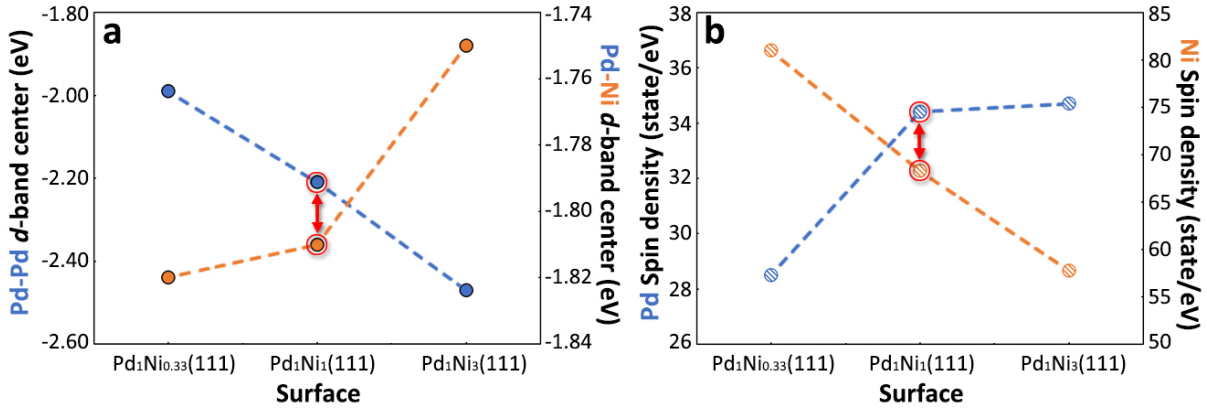

Fig. S9 a) *d*-band centers of Pd-Pd and Pd-Ni on $Pd_1Ni_x(111)$ surfaces and b) spin densities of Pd and Ni on each surface. Blue and orange circles represent values related to Pd and Ni, respectively. Red circles and arrows show that a balance point of activity exists. Among the surfaces, $Pd_1Ni_1(111)$ surface shows that there is a potential site where the electronic effects can be canceled out, that is, an adequate adsorption strength can be caused.

The band gaps discussed in the manuscript were calculated as the difference between d-band center values of Pd-Pd and Ni-Ni on $Pd_1Ni_{0.33}(111)$, $Pd_1Ni_1(111)$ and $Pd_1Ni_3(111)$ surfaces, respectively. For example, |Pd-d of $Pd_1Ni_{0.33}(111)$ – Ni-d of $Pd_1Ni_{0.33}(111)$| is |(–1.99 eV) – (–1.32 eV)| = 0.67 eV. The *d*-band centers of Ni-Ni on $Pd_1Ni_{0.33}(111)$, $Pd_1Ni_1(111)$ and $Pd_1Ni_3(111)$ surfaces are –1.32, –1.43 and –1.52 eV, respectively.

The electronic properties of each of Pd and Ni atom showed inverse tendency as the Ni content increased (Fig. S9). As the Ni content of the Pd-Ni alloys increases, the d-band center value of Pd decreases and that of Ni increases; on the other hand, the spin density of Pd increases and that of Ni decreases. This fact implies that the catalyst surface sites where strong and weak adsorption can occur coexist on the Pd-Ni alloy catalysts with minimum and maximum Ni contents (i.e., $Pd_1Ni_{0.33}(111)$ and $Pd_1Ni_3(111)$, respectively). In the case of the Pd-Ni alloy catalyst with a proper amount of Ni (i.e., $Pd_1Ni_1(111)$), a potential surface site may be formed where the inverse electronic effects can be canceled out, resulting in moderately strong or weak adsorption of adsorbates. Considering the fact that the strong adsorption strength of adsorbates is not unconditionally helpful to the catalytic activity, we propose an indirect indicator that an appropriate Ni content can induce an appropriate adsorption strength of the adsorbates, thereby enhancing catalytic activity.

Atomic hydrogen adsorption on Pd(111), Pd_1Ni_x(111) and Ni(111) surfaces

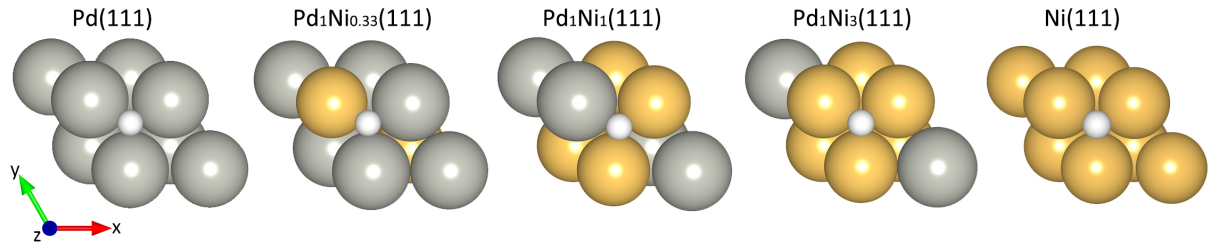

Fig. S10 Top views of Pd(111), Pd_1Ni_x(111) and Ni(111) surfaces with adsorbed hydrogen. Grey, yellow and white spheres represent Pd, Ni and H, respectively. Ni(111) surface has a hydrogen adsorption strength of –0.59 eV, which is a relatively stronger energy than those of $Pd_1Ni_{0.33}$(111) and Pd_1Ni_1(111) surfaces (Table S9) with the excellent efficiency of HCOOH dehydrogenation. These figures are part of Pd(111)-*p*(4×4), Pd_1Ni_x(111)-*p*(4×4) and Ni(111)-*p*(4×4) surfaces, respectively.

In order to calculate the adsorption energy of hydrogen atom on the Ni catalyst, we performed the optimization of bulk Ni and confirmed the lattice constant of 3.52 Å, which agreed well with the experimental (3.52 Å) and theoretical (3.52 Å) results (see reference [63] in the manuscript). Using this lattice constant, Ni(111)-*p*(4×4) surface was constructed and the adsorption energy of hydrogen atom was calculated by using the same calculation methods as used for the Pd(111) and Pd_1Ni_x(111) surfaces. The adsorption energies were 0.01, –0.44, –0.57 and –0.59 eV at atop, bridge, hollow (hcp) and hollow (fcc) sites, respectively. Like on other Pd_1Ni_x(111) surfaces, the hollow (fcc) site showed the most stable adsorption strength, which was particularly similar to that of Pd_1Ni_3(111) (–0.58 eV) surfaces. In the manuscript, we discussed that the adsorption strength of hydrogen atom is generally proportional to the activation energy of the rate determining step (in other words, the adsorption energy is inversely proportional to the activation energy in Fig. 8d in the manuscript). Therefore, it can be indirectly predicted that pure Ni catalyst may not have a positive effect on the HCOOH dehydrogenation efficiency in terms of prediction by hydrogen adsorption strength.

Single point calculations for atomic hydrogen desorption on Pd(111) and Pd_1Ni_x(111) surfaces

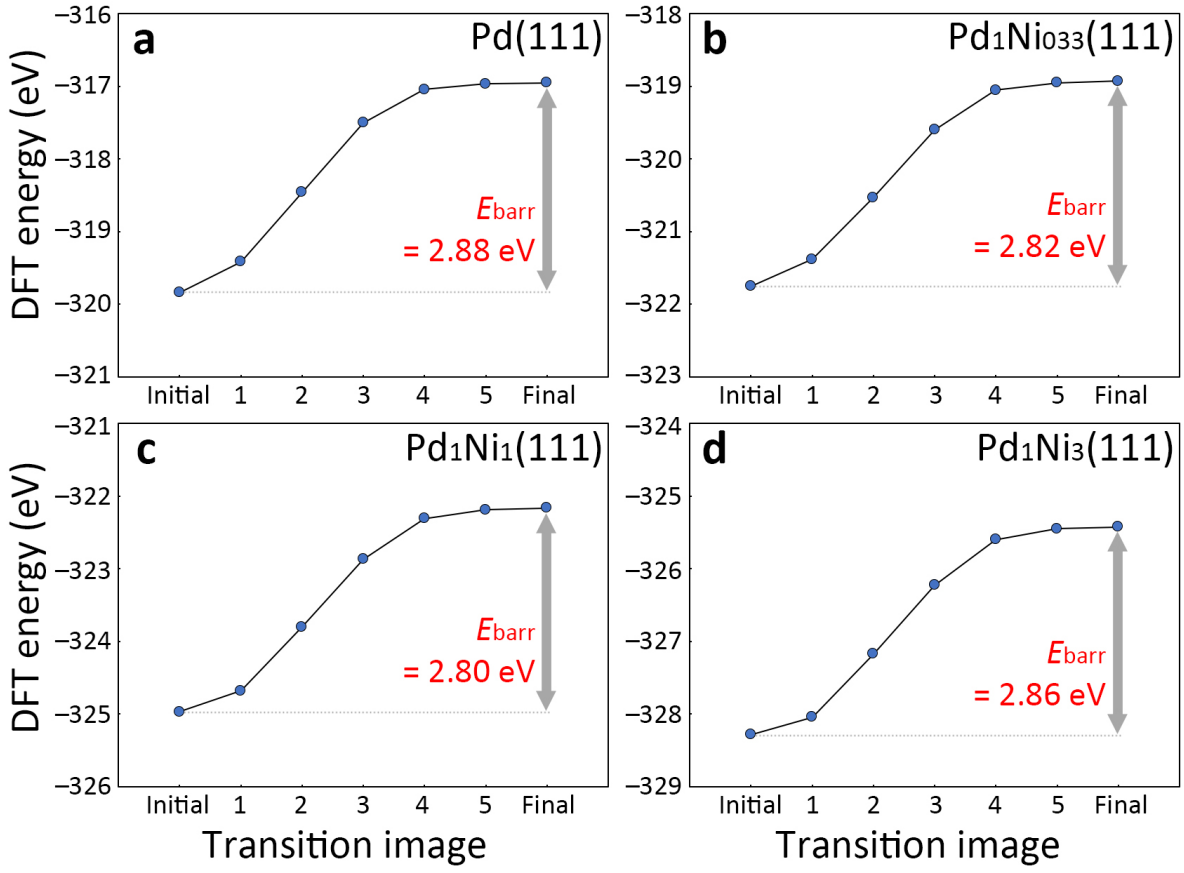

Fig. S11 Activation energy diagrams for the desorption of hydrogen. All calculations were performed by fixing both the surface and the adsorbate.

Calculations to check the validity of surface size and k-points

Table S6 Adsorption energies of HCOOH on Pd(111) and Pd_1Ni_1(111) surfaces of various sizes. Pd_1Ni_1(111)-*p*(6×6) surface was designed because it was unable to design (3×3) and (5×5) surfaces due to the Pd:Ni ratio. (4×4) surface was used in this study.

Surfaces	Adsorption energy of HCOOH (eV)			
	(3×3)	(4×4)	(5×5)	(6×6)
Pd(111)	–0.39	–0.40	–0.40	–
Pd_1Ni_1(111)	–	–0.46	–	–0.44

Table S7 Difference between activation energies (TS_3 (eV) (II →IV)) on Pd(111) and Pd_1Ni_1(111) surfaces depending on k-points.

k-points	Activation energy (eV)	
	Pd(111)	Pd_1Ni_1(111)
4 × 4 × 1	1.19	1.02
2 × 2 × 1	1.17	1.02

Bond lengths of gas-phase HCOOH, $HCOO_a$*, $HCOO_b$* and COOH*

Table S8 Calculated geometrical parameters of free HCOOH, HCOOH*, $HCOO_a$*, $HCOO_b$* and COOH* on Pd(111) and Pd_1Ni_x(111) surfaces.

Free/adsorb molecules		O–H (Å)	C–H (Å)	C=O (Å)	C–O (Å)
HCOOH		0.984	1.104	1.210	1.353
Pd(111)	HCOOH*	1.015	1.102	1.236	1.236
	$HCOO_a$*	-	1.110	1.270	1.269
	$HCOO_b$*	-	1.173	1.303	1.217
	COOH*	0.985	-	1.270	1.365
$Pd_1Ni_{0.33}$(111)	HCOOH*	1.034	1.100	1.238	1.312
	$HCOO_a$*	-	1.107	1.275	1.263
	$HCOO_b$*	-	1.182	1.307	1.214
	COOH*	0.989	-	1.262	1.342
Pd_1Ni_1(111)	HCOOH*	1.021	1.100	1.237	1.315
	$HCOO_a$*	-	1.107	1.269	1.271
	$HCOO_b$*	-	1.115	1.366	1.206
	COOH*	0.988	-	1.276	1.340
Pd_1Ni_3(111)	HCOOH*	1.024	1.097	1.241	1.315
	$HCOO_a$*	-	1.104	1.272	1.273
	$HCOO_b$*	-	1.162	1.310	1.219
	COOH*	0.987	-	1.275	1.345

Adsorption energy and work function

The adsorption energy (E_{ads}) is defined as $E_{ads} = E_{ad/slab} - (E_{slab} + E_{ad})$, where $E_{ad/slab}$, E_{slab} and E_{ad} are the total energies of the slab with adsorbate, the bare slab and a free adsorbate, respectively. Accordingly, negative values of E_{ads} represent exothermic (stable) adsorption (*i.e.*, the more negative E_{ads}, the stronger adsorption).

The work function(Φ) is the minimum energy required to extract an electron from a surface and is defined as $\Phi = V_{vac} - E_f$, where V_{vac} and E_f are the vacuum potential and the Fermi energy.

Table S9 The most stable adsorption energies (E_{ads}) of intermediate species produced during FA dehydrogenation over Pd(111), $Pd_1Ni_{0.33}$(111), Pd_1Ni_1(111) and Pd_1Ni_3(111) surfaces.

Adsorbate species	E_{ads} (eV)			
	Pd(111)	$Pd_1Ni_{0.33}$(111)	Pd_1Ni_1(111)	Pd_1Ni_3(111)
HCOOH*	–0.40	–0.79	–0.46	–0.62
$HCOO_a$*	–2.49	–3.15	–3.07	–3.35
$HCOO_b$*	–1.77	–2.45	–2.12	–2.38
COOH*	–2.21	–2.31	–2.45	–2.41
H*	–0.60	–0.52	–0.53	–0.58
CO*	–2.03	-	–1.92	-
OH*	–2.73	-	–3.38	-

Table S10 Adsorption energies (E_{ads}) of intermediate species produced during FA dehydrogenation over Pd(111) surface.

Adsorption sites	E_{ads} (eV)						
	HCOOH*	$HCOO_a$*	$HCOO_b$*	COOH*	CO*	H*	OH*
1	–0.40	–2.49	–1.77	–2.15	–1.38	–0.04	–1.71
2	–0.23	–2.46	–1.66	–2.21	–1.82	–0.48	–2.47
3	–0.17	–2.49	–1.74	–2.18	–1.78	–0.56	–2.55
4	–0.19	–	–1.67	–2.18	–2.03	–0.60	–2.73

Table S11 Adsorption energies (E_{ads}) of intermediate species produced during FA dehydrogenation over $Pd_1Ni_1(111)$ surface.

Adsorption sites	E_{ads} (eV)						
	HCOOH*	HCOOa*	HCOOb*	COOH*	CO*	H*	OH*
1	–0.37	–2.51	–1.78	–2.04	–1.21	–0.07	–2.34
2	–0.46	–3.07	–2.12	–2.42	–1.64	–0.48	–2.47
3	–0.21	–2.52	–1.72	–2.06	–1.53	–0.31	–2.44
4	–0.36	–2.99	–2.07	–1.77	–1.72	–0.49	–3.02
5	–0.31	–3.07	–2.10	–2.44	–1.88	–0.53	–3.38
6	–0.36	–3.05	–2.09	–2.39	–1.89	–0.49	–3.26
7	–0.46	–2.90	–2.05	–1.98	–1.88	–0.48	–2.93
8	–0.32	–3.07	–1.92	–2.45	–1.92	–0.53	–3.37
9	–0.41	–3.02	–2.01	–2.20	–1.82	–0.49	–3.01

Table S12 Adsorption energies (E_{ads}) of HCOOH*, $HCOO_a$*, $HCOO_b$* and COOH* on $Pd_1Ni_{0.33}(111)$ and $Pd_1Ni_3(111)$ surfaces.

Adsorption sites	E_{ads} (eV)							
	$Pd_1Ni_{0.33}(111)$				$Pd_1Ni_3(111)$			
	HCOOH*	$HCOO_a$*	$HCOO_b$*	COOH*	HCOOH*	$HCOO_a$*	$HCOO_b$*	COOH*
3	–0.37	–2.81	–2.12	–2.06	–0.62	–3.35	–2.38	–2.41
4	–0.33	–3.15	–2.44	–2.14	–0.41	–3.29	–2.37	–2.38
5	–0.79	–3.15	–2.45	–2.31	–0.31	–3.08	–2.02	–2.21

Table S13 Adsorption energies (E_{ads}) of H* on $Pd_1Ni_{0.33}(111)$ and $Pd_1Ni_3(111)$ surfaces.

Adsorption sites	E_{ads} H*(eV)	
	$Pd_1Ni_{0.33}(111)$	$Pd_1Ni_3(111)$
1	–0.04	–0.12
2	–0.02	–0.58
3	–0.38	–0.44
4	–0.35	–0.49
5	–0.05	–0.33
6	–0.44	–0.51
7	–0.48	–0.49
8	–0.50	–0.58
9	–0.52	–0.49

Activation energies of key reaction steps on $Pd_1Ni_{0.33}$(111) and Pd_1Ni_3(111) surfaces

Table S14 Calculated activation energies for FA dehydrogenation through the optimal steps in HCOO pathway and the initial step in COOH pathway. Refer to the illustration and notation in Fig. 5 for the intermediate species marked as I ~ VI and TS_1 ~ TS_7.

Surface	HCOO pathway			COOH pathway
	TS_1 (eV) (I →II)	TS_3 (eV) (II →IV)	TS_4 (eV) (IV→III)	TS_5 (eV) (I→V)
$Pd_1Ni_{0.33}$(111)	0.77	0.86	0.22	0.78
Pd_1Ni_3(111)	0.60	1.16	-	0.74

Electronic and geometric effects

Based on adsorption energies on Pd(111) and Pd_1Ni_x(111) surfaces, we assumed that the electronic (E_{elec}) and geometric (E_{geo}) effects are defined as $E_{elec} = E_{PdNi} - E_{Pd(comp)}$ and $E_{geo} = E_{Pd(comp)} - E_{Pd}$, where E_{PdNi}, $E_{Pd(comp)}$ and E_{Pd} are adsorption energies of adsorbates on Pd_1Ni_x(111), Pd(111) with compressive strain (2.00, 5.48 and 7.70) and Pd(111) surfaces.

Table S15 Energies assumed to be electronic (E_{elec}) and geometric (E_{geo}) effects caused by the formation of Pd_1Ni_x alloys.

Adsorbate species		$Pd_1Ni_{0.33}$(111)		Pd_1Ni_1(111)		Pd_1Ni_3(111)	
		ΔE (eV)	Percentage (%)	ΔE (eV)	Percentage (%)	ΔE (eV)	Percentage (%)
HCOOH*	E_{elec}	–0.42	107.0	–0.15	225.3	–0.33	147.6
	E_{geo}	0.03	–7.0	0.08	–125.3	0.11	–47.6
HCOOa*	E_{elec}	–0.71	107.4	–0.74	127.6	–1.12	130.6
	E_{geo}	0.05	–7.4	0.16	–27.6	0.26	–30.6
HCOOb*	E_{elec}	–0.72	105.8	–0.49	137.4	–0.84	136.2
	E_{geo}	0.04	–5.8	0.13	–37.4	0.22	–36.2
COOH*	E_{elec}	–0.16	161.4	–0.40	169.8	-	-
	E_{geo}	0.06	–61.4	0.16	–69.8	-	-
H*	E_{elec}	0.05	–56.8	–0.08	101.9	–0.20	896.8
	E_{geo}	0.04	–43.2	0.15	–201.9	0.22	–996.8

Table S16 Adsorption energies (E_{ads}) of key intermediate species on Pd(111) surfaces with compressive strain.

Adsorbate species	E_{ads} (eV)		
	2.00 %	5.78 %	7.70 %
HCOOH*	–0.37	–0.31	–0.29
$HCOO_a$*	–2.44	–2.33	–2.23
$HCOO_b$*	–1.73	–1.64	–1.55
COOH*	–2.15	–2.05	-
H*	–0.57	–0.45	–0.38

References

[S1] Ö. Metin, X. Sun and S. Sun, *Nanoscale*, 2013, **5**, 910–912.

[S2] J. L. Santos, C. León, G. Monnier, S. Ivanova, M. Á. Centeno and J. A. Odriozola, *Int. J. Hydrog. Energy*, 2020, **45**, 23056-23068.

[S3] S. Zhang, O. Metin, D. Su and S. Sun, *Angew. Chem. Int. Ed.*, 2013, **52**, 3681.

[S4] Z. Zhang, Y. Luo, S. Liu, Q. Yao, S. Qing and Z. Lu, *J. Mater. Chem. A*, 2019, **7**, 21438-21446

[S5] Y. Qin, J. Wang, F. Meng, L. Wang and X. Zhang, *Chem. Commun*., 2013, **49**, 10028−10030.

[S6] W. Nie, Y. Luo, Q. Yang, G. Feng, Q. Yaoa and Z. Lu, *Inorg. Chem. Front*., 2020, **7**, 709–717.

[S7] I. Barloccoa, S. Capelli, E. Zanella, X. Chen, J. J. Delgado, A. Roldan, N. Dimitratos and A. Villa, *J. Energy Chem.*, 2021, **52**, 301–309.

[S8] A. Bulut, M. Yurderi, Y. Karatas, M. Zahmakiran, H. Kivrak, M. Gulcan and M. Kaya, *Appl. Catal. B Environ.*, 2015, **164**, 324-333.

[S9] M. Yurderi, A. Bulut, M. Zahmakiran and M. Kaya, *Appl. Catal. B Environ.*, 2014, **160-161**, 514-524.

[S10] D. Y. Shin, M.-S. Kim, J. A. Kwon, Y.-J. Shin, C. W. Yoon and D.-H. Lim, *J. Phys. Chem. C*, 2019, **123**, 1539-1549.